PHOTONICS Research

Frequency comb swept laser with a high-Q microring filter

Dongmei Huang,[1,2] Feng Li,[1,2,*] Chao Shang,[2,3] Zihao Cheng,[1,2] S. T. Chu,[4] and P. K. A. Wai[1,2]

[1]Photonics Research Centre, Department of Electronic and Information Engineering, The Hong Kong Polytechnic University, Hong Kong SAR, China
[2]The Hong Kong Polytechnic University Shenzhen Research Institute, Shenzhen 518057, China
[3]Photonics Research Centre, Department of Electrical Engineering, The Hong Kong Polytechnic University, Hong Kong SAR, China
[4]Department of Physics and Materials Science, City University of Hong Kong, Hong Kong SAR, China
*Corresponding author: enlf@polyu.edu.hk

Received 30 December 2019; revised 21 March 2020; accepted 24 March 2020; posted 24 March 2020 (Doc. ID 386900); published 19 May 2020

Frequency comb swept lasers are the enabling technology of circular interferometric imaging, which was proposed to break the bottleneck of data acquisition and processing in optical coherence tomography (OCT) at video rate. In this paper, we propose and demonstrate a highly coherent frequency comb swept laser by using a high-quality (high-*Q*) microring comb filter to discretize a Fourier-domain mode-locked (FDML) laser. The microring filter has a *Q* factor of ~2×10^6 and a linewidth of ~90 MHz. To demonstrate the improvement in performance, a Fabry–Pérot comb filter with a *Q* factor of 6.2×10^4 and a linewidth of 3.1 GHz is also used in the experiment for comparison. Both comb filters have free spectral ranges (FSRs) of ~50 GHz for consistence. Stable and clearly discretized temporal waveforms and frequency comb spectra with 50 GHz FSR are observed. Adoption of the high-*Q* microring filter narrows the instantaneous linewidth of the FDML laser down to 1.5 GHz. The OCT system with the frequency comb swept laser source with a microring filter demonstrates an ultralong imaging range, which has a 6, 10, and 15 dB sensitivity roll-off length of ~53, ~73, and over 100 mm, respectively.

https://doi.org/10.1364/PRJ.386900

1. INTRODUCTION

Swept laser sources have extensive applications in optical devices and sub-system testing, fiber characterization, optical sensing including fiber Bragg grating (FBG) interrogation, and most importantly in optical coherence tomography (OCT) systems [1–5]. Swept source OCT (SS-OCT) is the most promising OCT technique in development to realize volumetric biomedical imaging at video rate [6–9]. Compared with time-domain OCT (TD-OCT), which is hampered by the slow mechanical movement of the reference mirror, and spectral-domain OCT (SD-OCT), which is limited by resolution and the low acquisition rate of the spectrometer, SS-OCT could provide much higher axial scan (A-scan) rate owing to the motionless interferometer structure and the sophisticated high-speed photodetectors widely used in optical communications [7,10]. The core technology of the SS-OCT system is the swept laser source, the sweep rate, sweep range, and instantaneous linewidth of which directly determine the imaging performance.

In a conventional tunable-filter-based short-cavity swept laser, when the transmission wavelength of the tunable filter is changed, the build-up time of the laser oscillation at the new wavelength limits the tuning speed and hence the sweep rate [11]. In 2006, Huber *et al.* proposed a Fourier-domain mode-locked (FDML) laser with a long fiber ring cavity, which avoided the limitation imposed by laser build-up from spontaneous emission and increased the sweep rate to nearly 300 kHz [4]. Although the sweep rate of FDML lasers in principle could be very high, it is limited to hundreds of kilohertz in experiments by the resonant frequency of the piezo-driven optical tunable filter. When used in conjunction with a buffer scheme, the sweep rate can be boosted to several megahertz (MHz) [12–14]. Besides the high sweep rate, FDML lasers could provide a sweep range of >120 nm by using a single semiconductor optical amplifier (SOA) [15] or a sweep range of >280 nm if two SOAs at 1310 nm and 1500 nm are jointly used in the cavity [16], which leads to very high axial resolutions in OCT systems [16]. However, conventional FDML lasers do not provide much enhancement on the instantaneous linewidth or the coherence length of the swept signal, which limits the imaging range of OCT systems to a few millimeters, or slightly longer than 10 mm if dispersion compensation is carefully adopted [17,18].

It has been demonstrated in both simulations and experiments that the output of FDML lasers suffers from a strong high-frequency modulation on the waveforms, which degrades

the signal quality and the coherence length. The high-frequency fluctuations are due to the residual chromatic dispersion, which can be eliminated by active precise chromatic dispersion compensation with feedback [19]. In a cavity with residual chromatic dispersion, both the sweep frequency detuning and the nonlinearities of the fiber and SOAs will jointly introduce a time-dependent relative frequency deviation to the swept signal from the sweep trace of the tunable filter. When the frequency offset accumulates to sufficiently large, it will trigger the Eckhaus instability and generate sidebands leading to the high-frequency fluctuations on the waveforms [20]. The new sidebands, which are close to the filter center, will be amplified but will be detuned away from the filter center again in multiple round-trips. The repetitive triggering of the Eckhaus instability will intrinsically limit the minimal instantaneous linewidth [20].

Much effort has been made to enhance the coherence length of swept lasers and the imaging range of OCT systems with such sources. Researchers encounter another bottleneck in the quest to improve the performance of swept sources for OCT systems. The digitization rate and data transfer speed are often insufficient for real-time OCT, which may limit the frame rate and the imaging range of OCT with high axial resolution and high A-scan rate [21]. In 2018, Siddiqui *et al.* demonstrated that a circular interferometric ranging scheme could multiply the imaging range without increasing the computation requirement [6,22]. A frequency comb swept laser is used as the source of such circular interferometric ranging system. An extra benefit of using such frequency comb swept laser is the increase in the coherence length. It has been demonstrated that such discretization of FDML laser with a Fabry–Pérot (F–P) comb filter is an effective method to enhance the coherence length [23–26]. However, limited by the relatively low finesse of the F–P filter, the roll-off length of OCT with such discrete swept source is only at the level of ~10 mm [23].

Compared with fiber F–P comb filters, high-quality (high-Q) whispering-gallery mode (WGM)-based microcavity filters could provide much higher finesse and narrower linewidth. Nowadays, a crystalline micro-disk could have a Q factor of $\sim 10^{11}$ [27]. But the coupling from a fiber to the crystalline microcavities is unstable and remains very challenging. In the last decade, the development of state-of-the-art optical waveguide techniques has enabled the fabrication of waveguide-coupled microrings with Q factors $>10^6$ in multiple platforms [28–34]. In this paper, we propose and experimentally demonstrate a highly coherent frequency comb swept laser by discretizing an FDML laser with an on-chip Hydex glass microring filter with a Q factor of $\sim 2 \times 10^6$. The experimental setup will be shown in Section 2. We will discuss the results including the output spectra, waveforms, and the point spread functions (PSFs) of the OCT system compared with a discrete FDML laser with an F–P comb filter in Section 3. Section 4 will give the conclusions.

2. EXPERIMENTAL SETUP

Figure 1 shows the schematic diagram of the FDML laser with a comb filter (microring or F–P comb filter) in the cavity. Two SOAs (Thorlabs, BOA1004S) with a 3 dB amplified

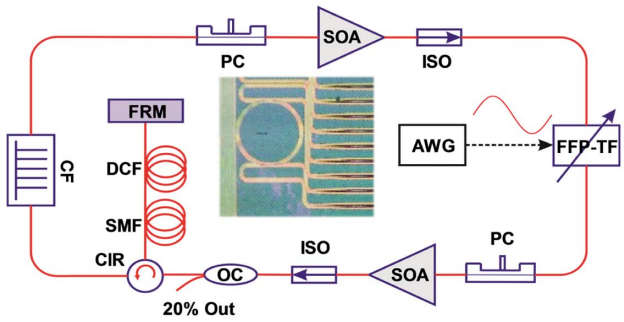

Fig. 1. Schematic diagram of an FDML laser with a comb filter. FFP-TF, Fiber Fabry–Pérot tunable filter; SOA, semiconductor optical amplifier; ISO, isolator; AWG, arbitrary-waveform generator; OC, optical coupler; PC, polarization controller; CIR, circulator; SMF, single-mode fiber; DCF, dispersion compensation fiber; FRM, Faraday rotating mirror; CF, comb filter (microring or F–P comb filter). The inset shows a photo of the Hydex glass microring comb filter.

spontaneous emission (ASE) bandwidth of 85 nm, small signal gain of 27 dB, and saturation output power of 15 dBm serve as the gain elements in the cavity. The wavelength sweep is realized by a fiber F–P tunable filter (FFP-TF, Micron Optics) with a free spectral range (FSR) of 25 THz and a linewidth of 16 GHz. A section of double-pass optical fiber 2120 m long, which consists of 1916 m of single-mode fiber (SMF, G.652D) and 204 m of dispersion compensation fiber (DCF, OFS), is incorporated into the laser cavity to match the resonant-driven frequency of the FFP-TF and reduce the cavity dispersion. A sinusoidal electrical signal generated by an arbitrary-waveform generator (AWG, Keysight, 33622A) is applied to the piezoelectric transducer (PZT)-driven FFP-TF. When the driving frequency is tuned to the resonant frequency of the FFP-TF, which is the fundamental resonant frequency of the fiber cavity, the swept lasing signal can be stored in the long fiber cavity and repeatedly pass through the swept filter without the need to rebuild from ASE. To eliminate the polarization-mode dispersion induced by the linear birefringence of the long fiber and shorten the physical fiber length, a Faraday rotating mirror (FRM) combined with a circulator (CIR) is applied to route the light to double pass the long optical fiber. Isolators (ISOs) are utilized to block the reflected light to guarantee the stability of the SOAs. In addition, polarization controllers (PCs) are used to adjust the polarization states of the light injected into the SOAs and the microring filter to reduce the polarization-dependent loss. At the output optical coupler (OC), 20% of the signal is exported and sent to the optical spectrum analyzer (OSA) and oscilloscope (OSC) to characterize the swept signal. A comb filter (CF), either a microring filter or an F–P filter for comparison, is used in the cavity to slice the swept signal in the frequency domain as well as to chop the swept signal into discrete pulses in the time domain, which will improve the coherence length of the swept signal.

In the experimental setup shown in Fig. 1, the comb filter is a key component to control the performance of the output signal. With an F–P comb filter, the roll-off length of the OCT system with FDML laser could be enhanced from a few millimeters to ~10 mm. To further narrow the linewidth

of the output signals, comb filters with a higher Q factor should be adopted. In the last two decades, WGM-based microresonators have attracted much attention owing to the ultrahigh Q factors they have demonstrated and successful generation of Kerr frequency comb and cavity solitons [27,32–35]. The application of microresonators to discrete FDML lasers does not require the highest Q factor achievable. A Q factor of $\sim 10^6$, which corresponds to a filter linewidth of several hundreds of megahertz (MHz), is the optimum choice. A higher filter Q factor will lead to a longer pulse for each discrete channel. Too high a Q factor may cause overlap of adjacent pulses. Thus, crystalline microcavities are not considered here because their ultrahigh Q factors are not needed, and coupling to these microcavities is unstable [27]. Hydex glass is an excellent material that shows simultaneous low nonlinearity and low absorption [32]. On-chip Hydex glass microcavities could show a loaded Q factor of $>10^6$ and a linewidth of <200 MHz for individual comb lines [30–32]. In this paper, a Hydex glass microring resonator with a Q factor of $\sim 2 \times 10^6$ and an FSR of 50 GHz is chosen as the comb filter. A photo of the microring resonator is shown in the inset of Fig. 1. For a frequency comb swept laser, the FSR of discrete comb lines is inversely proportional to the period of the Fourier transform, and an FSR of 50 GHz will induce a period of 3 mm for circular interferometric imaging [6]. The FSR could be reduced to enlarge the imaging period. It has been demonstrated in simulation that an FSR of 50 GHz will help avoid overlap of pulses from adjacent frequency channels [36].

To characterize the performance of the frequency comb swept lasers, the PSFs are measured at different positions with a Michelson interferometer scheme as shown in Fig. 2. The output swept signal from the swept source is divided into two parts by an optical coupler. Eighty percent of the discrete swept signal is detected by a photodetector and recorded by the oscilloscope as the clock signal to be used in the self-clocking calibration. At the same time, 20% of the swept signal is sent to the Michelson interferometer. Two motorized reflective variable optical delay lines (VODLs) with two circulators and two PCs are used as the two arms. The interference signals

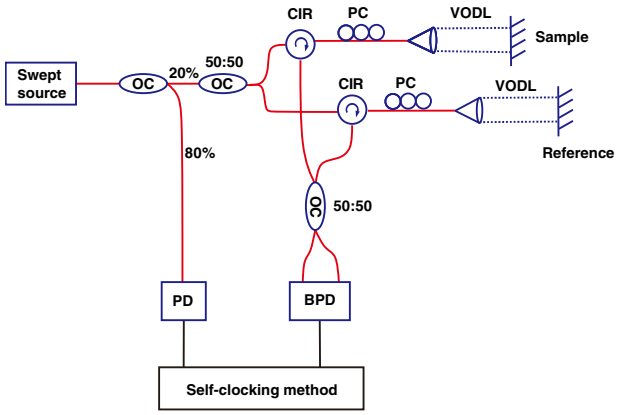

Fig. 2. Schematic diagram of the point spread function and sensitivity roll-off measurement system. OC, optical coupler; PD, photodetector; BPD, balanced photodetector; CIR, circulator; PC, polarization controller; VODL, variable optical delay line.

combined in the 50:50 coupler are detected by a 43 GHz balanced photodetector (BPD, Finisar, BPDV2150R) and then are acquired by a high-speed real-time oscilloscope (Keysight, MSOS404A) with a bandwidth of 4 GHz and a sampling rate of 20 GSa/s. Assisted by the clock signal from the PD, the interference signal is resampled in time domain, and the resampled signal is already a uniformly sampled spectrum in frequency domain. The PSFs can be obtained by Fourier transform of the interference spectra. The instantaneous linewidth or the coherence length of the swept laser can be estimated by measuring the sensitivity roll-off, which can be obtained by tuning the delays between the sample and reference arms.

It should be noted that the number of sampling points is determined by the sweep range and FSR of the comb filter. The discrete sampling with a frequency interval of 50 GHz will lead to a period of $X_p \sim 3$ mm in circulating imaging [6]. The PSF peaks for the samples at distances $z = x + nX_p > 0$, where n is a natural number and $x \in [-X_p/2, X_p/2]$, will all appear at the position x of the PSF window of the Fourier transform. To characterize the coherence length and sensitivity roll-off of the OCT, we unwrap the circulating PSFs with assistance of the positions of the VODLs.

3. EXPERIMENTAL RESULTS AND DISCUSSION

In this section, we will first compare the properties of the microring and F–P comb filters used in the discrete FDML lasers. Thereafter, the output spectra and waveforms of the frequency comb swept lasers will be shown and analyzed. The frequency comb swept lasers with the F–P and microring filters are then used in the OCT system, and the sensitivity roll-off is characterized by measuring a series of PSFs.

A. Microring and F–P Comb Filters

It is clear the Q factor of the comb filter is a key parameter that affects the performance of FDML lasers. In the experiment, we use two different comb filters with different Q factors. The F–P comb filter is fabricated by a highly reflective multilayer dielectric coating on both surfaces of a two-side polished fused silica substrate with a thickness of 2 mm. The coated substrate is then sliced into 2 mm × 2 mm × 2 mm cubes and packaged with a pair of fiber collimators. The packaged F–P comb filter has an FSR of ~50 GHz and a finesse of ~17. To obtain a stable linear high-Q comb filter, we use a Hydex glass on-chip microring filter. Hydex glass has a refractive index between 1.5 and 1.9 [32]. It is convenient to fabricate ridge waveguides by etching the Hydex glass film on a silica substrate and then coating the waveguide by silica for protection and dispersion engineering. By virtue of the lower refractive index than Si and SiN, the size of the Hydex glass waveguide is much larger than that of Si and SiN waveguides, which alleviates the difficulty of fabrication. Sliced SMFs are used to couple light to and from the waveguide directly with a total coupling loss <4 dB owing to the large core size and low numerical aperture of the Hydex glass waveguide. To be consistent, the FSR of the microring comb filter is also designed to be ~50 GHz. To characterize the performance of the microring and F–P comb filters in the spectral region of the FDML laser, the ASE of one of the two SOAs is used as the source. The transmission spectra of both filters are measured by

an optical complex spectrum analyzer (OCSA, APEX, AP2441A) with 20 MHz resolution.

Figure 3 shows the spectra captured by the OCSA with averaging of 30 measurements. From Figs. 3(a) and 3(b), the FSR of the microring comb filter is 50 GHz, and both the TE and TM modes are excited in the microring resonator. By Lorentzian fitting, shown in Figs. 3(c) and 3(d), the full widths at half-maximum (FWHMs) of the TM and TE modes are 96 MHz and 88 MHz, respectively. Both modes have Q factors of $\sim 2.0 \times 10^6$. In the characterization, both the TE and TM modes are excited since we use an unpolarized ASE source. The TE and TM modes can be selectively excited in a laser cavity when a polarization controller is utilized to adjust the polarization state of light injected into the microring filter. Figure 3(e) shows the transmission spectrum of the F–P comb filter. Figure 3(f) shows the fine structure of a single resonance. The FSR is measured to be 50 GHz and the FWHM is 3.1 GHz, corresponding to a Q factor of 6.2×10^4, which is significantly lower than that of the microring filter. From Fig. 3, the two comb filters have similar contrast ratios of ~20 dB on the transmission spectra.

B. Frequency Comb Swept Lasers with Different Comb Filters

The two characterized comb filters are then separately utilized in the FDML laser cavity shown in Fig. 1 to obtain frequency comb swept laser signals. In the experiments, stable and clearly discretized waveforms in the time domain and frequency comb

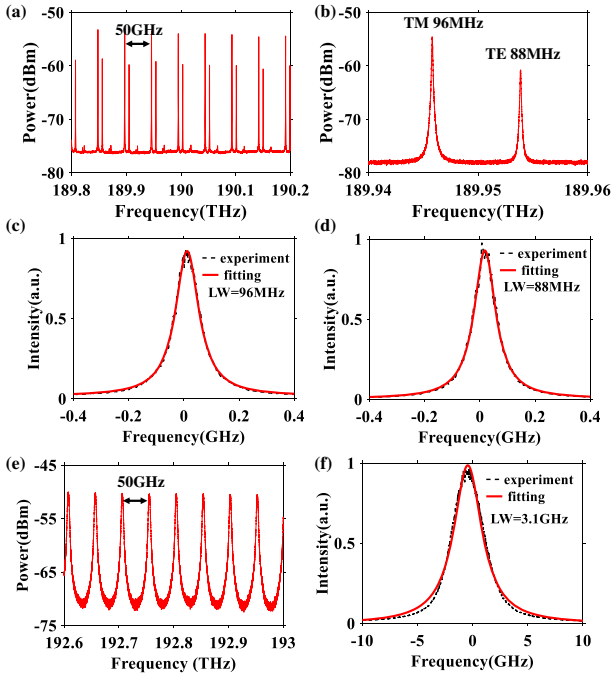

Fig. 3. (a) Transmission spectrum of the microring filter. (b) The fine structures of a pair of resonances for TE and TM modes; (c) and (d) respectively show the TM and TE resonances shown in (b) with Lorentzian fittings. (e) Transmission spectrum of the F–P comb filter. (f) The fine structure of one resonance of the F–P comb filter with Lorentzian fitting. All the spectra are captured with averaging of 30 measurements.

with 50 GHz FSR in the frequency domain are observed with either of the two comb filters. Discretization of the FDML laser with a comb filter will effectively improve the coherence length and narrow the instantaneous linewidth of the swept laser [23]. From our demonstration in Ref. [36], a comb filter with higher finesse or narrower linewidth will improve the quality of the swept signal with less noise and further increase the coherence length. Figures 4 and 5 depict the output performance of frequency comb swept signals with the F–P and microring comb filters, respectively.

In the laser cavity, swept signals are sliced into discrete comb lines in the frequency domain with identical spacing defined by the FSRs of the comb filters. We first use the F–P comb filter in the FDML laser cavity. To match the 4266 m cavity length, the FFP-TF is driven by a 47.852 kHz sinusoidal signal, which corresponds to a round-trip time of 20.9 μs. Figures 4(a) and 4(b) show the optical spectra of the frequency comb swept signal with the F–P comb filter captured by an OSA (Yokogawa, AQ6370D) with different spectral spans. The spectrum of the frequency comb swept laser ranges from 1487 to 1618 nm with an identical wavelength separation of ~0.4 nm, covering a total tuning range of 131 nm. The slight intensity modulation on the spectrum is caused by the polarization-dependent gain of the SOA. Such intensity variation is hard to be fully eliminated in such a broad spectral range by adjusting the polarization controllers only. The background ASE noise limits the contrast ratio to ~20 dB in the central region and more than 30 dB in the side regions. In Fig. 4(c), we use the OCSA with 20 MHz resolution to measure the fine structure of a single comb line, which is selected out from the whole spectrum by a tunable filter (Santec, OTF-930) with a 3 dB bandwidth of 0.3 nm. By Lorentzian fitting, the linewidth of a single comb line of the frequency comb swept signal is 12.1 GHz. It should be noted that the linewidths vary slightly for different comb lines. Besides the spectral slicing, the comb filter will also chop the temporal waveform into a sequence of pulse trains, which has varying temporal separations since the sweep trace is nonlinear. Figure 4(d) shows the temporal waveform containing two full periods of sweep. Figure 4(f) shows the detail of the waveform within a time window of 300 ns. The waveform shows dense high frequency fluctuations, which will certainly degrade the signal quality and limit the coherence length. The details of the waveform or the fluctuations vary significantly for different pulses in the swept signal. The intensity fluctuations and the variations clearly indicate the residual chromatic dispersion of the cavity, which leads to the triggering of Eckhaus instability when coupled with the nonlinearity of the cavity. To observe the envelope of the pulses, we show the averaged waveform in 10 measurements in Figs. 4(e) and 4(g). It is clear that the pulse quality is greatly enhanced since the random high-frequency fluctuations are averaged out.

The microring comb filter with a Q factor of 2×10^6 is then incorporated into the FDML laser cavity to replace the F–P comb filter. It is expected that the linewidth of the frequency comb swept signal will be narrowed with the replacement. Because of the longer fiber tails of the microring filter, the resonant sweep rate corresponding to the cavity length is slightly decreased to 47.845 kHz. Figure 5 shows the output spectra

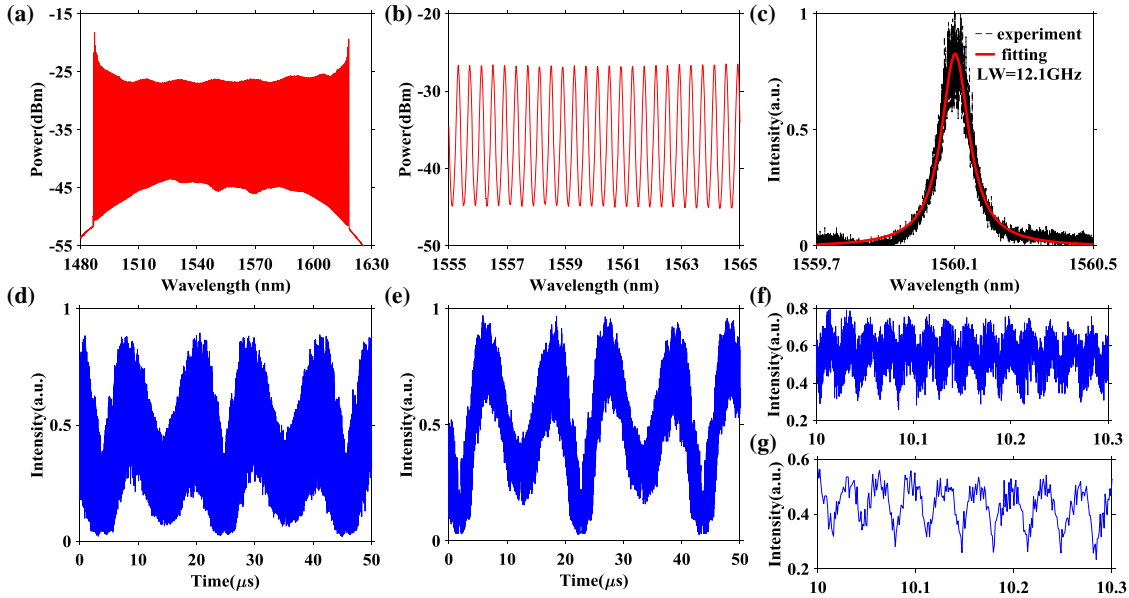

Fig. 4. Performance of a discrete FDML laser with F–P comb filter. (a) Output spectra and (b) the zoom-in view from 1555 to 1565 nm. (c) The instantaneous linewidth of the swept signal with Lorentzian fitting measured by the optical complex spectrum analyzer, (d) the temporal waveform, and (f) the zoom-in view from 10 to 10.3 μs without averaging. (e) The temporal waveform and (g) the zoom-in view with averaging of 10 measurements.

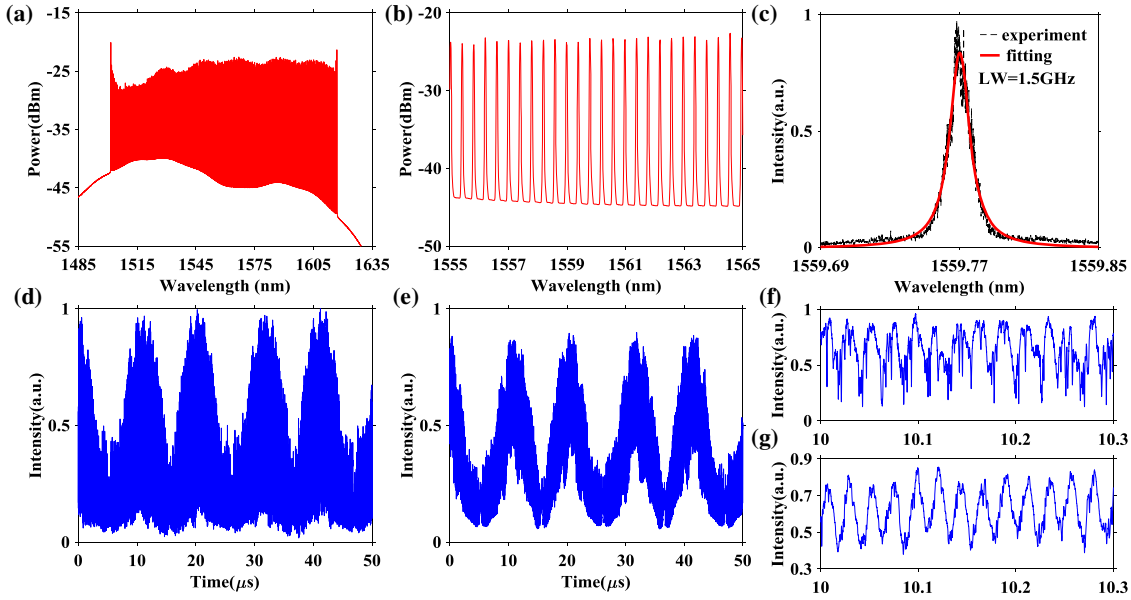

Fig. 5. Performance of the discrete FDML laser with microring comb filter. (a) The output spectra and (b) the zoom-in view from 1555 to 1565 nm. (c) The instantaneous linewidth of the swept signal with Lorentzian fitting measured by the optical complex spectrum analyzer, (d) the temporal waveform, and (f) the zoom-in view from 10 to 10.3 μs without averaging. (e) The temporal waveform and (g) the zoom-in view with averaging of 10 measurements.

and corresponding temporal waveforms. In Fig. 5(a), the sweep range of the frequency comb swept laser with the microring comb filter is 115 nm. The channel separation is 0.4 nm, corresponding to a filter FSR of 50 GHz. The sweep range is slightly decreased to match the net gain bandwidth of the cavity, which is decreased since the insertion loss of the microring comb filter is larger than that of the F–P filter. It can be observed in Fig. 5(b) that the comb lines are very narrow. Figure 5(c) shows the fine structure of a single comb line captured by the OCSA with a Lorentzian fitting. The linewidth is measured to be 1.5 GHz, which is only ∼1/8 of the linewidth with the F–P filter.

Figures 5(d) and 5(f) show the single trace waveform of the frequency comb swept signal with the microring comb filter

with different time windows for better observation of the envelope and details. Compared with the results with the F–P comb filter, Fig. 5(f) shows a clearer temporal waveform and a significant suppression of the high-frequency fluctuations benefiting from the narrower linewidth of the microring comb filter. The averaged waveforms shown in Figs. 5(e) and 5(g) show better quality than those in Fig. 4 too. Such improvement in the signal quality will enhance the performance of OCT systems.

C. Sensitivity Roll-Off Estimation of OCT Systems with Frequency Comb Swept Lasers

The coherence length or instantaneous linewidth of swept lasers can be characterized by measuring the sensitivity roll-off of the OCT. The coherence length of swept sources, which is twice the sensitivity roll-off length [17], can be estimated by the optical path difference between the two arms when the PSF peak drops by 6 dB. The variation of PSFs measured with a mirror located at different distances will illustrate the sensitivity roll-off of the OCT system. In principle, the interference fringes can be captured by the BPD when the sample arm is tuned to different distances as shown in Fig. 2. Then the PSFs can be obtained by Fourier transforms of the different interference fringes.

But in realization, the raw interference fringe signal captured by the BPD cannot be used to perform the Fourier transform directly since the discrete signal is not uniformly distributed in the time domain, which can be observed from the example shown in Fig. 6(a). Frequency comb swept lasers have an obvious advantage to realize a self-clocking calibration to convert the temporal waveforms into frequency spectra ready for Fourier transforms. In the experiment, the pulse train signals detected by the PD are not used as clock signal directly since there is too much noise on the waveforms. We extract the clock signal by removing the slowly varying and DC component by a high-pass filter and then removing the noisy intensity fluctuations by a low-pass filter. The interference fringe signal as shown in Fig. 6(a) is also filtered to remove the high-frequency noise and then resampled according to the peak positions of the clock signal. Figure 6(b) shows the resampled signal, which is uniformly distributed in the frequency domain. In the processing of the resampled signal, it was found that the spectral modulation inherited from the input signal, which has been observed in Figs. 4(a) and 5(a), will lead to side lobes on the PSFs. The side lobes are suppressed by applying a predefined complex modulation on the resampled signal with a Hann window. The signals are then ready to be used in fast Fourier transform (FFT) to obtain the PSFs.

By FFT of the resampled interference fringe signal, we can obtain the PSF as shown in Fig. 6(c), whose position directly indicates the position of the sample. The axial resolution of the OCT, i.e., the FWHM of the PSF, is measured to be 20 μm with a Gaussian fitting. Multiple PSFs for the OCT system with the frequency comb swept laser based on the F–P comb filter with different delays between the reference arm and the sample arm are shown in Fig. 6(d). As mentioned in Section 2, the frequency comb swept lasers will have a circulating imaging with a period determined by the FSR. To characterize the roll-off length, we should unwrap the circulating PSFs into the

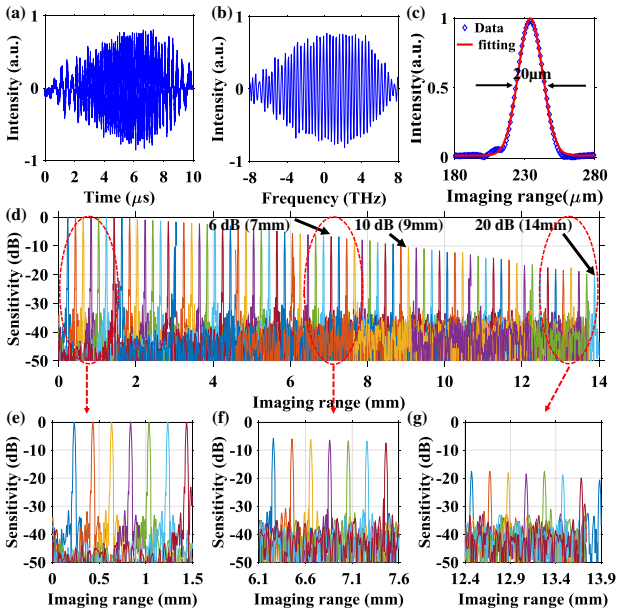

Fig. 6. (a) Example of raw interference fringe pattern with an F–P comb filter captured by the BPD. (b) Resampled interference spectrum with self-clocking. (c) Axial resolution estimation with PSF calculated from the signal of (b). (d)–(g) The measured PSFs of the frequency comb swept laser with an F–P comb filter for different OCT imaging ranges. (d) The imaging range from 0 to 14 mm. (e) The zoom-in view from 0 to 1.5 mm. (f) The zoom-in view from 6.1 to 7.6 mm, covering the 6 dB sensitivity roll-off length. (g) The zoom-in view from 12.4 to 13.9 mm, covering the 20 dB sensitivity roll-off length.

physical map with the relation $z = x + nX_p$ and make use of the reading of VODL positions. For the comb filters with an FSR of 50 GHz, the period X_p is ~3 mm. Figure 6(d) shows the unwrapped PSFs. From Fig. 6(d), the 6, 10, and 20 dB sensitivity roll-off lengths of the OCT system with frequency comb swept lasers based on the F–P comb filter are 7, 9, and 14 mm, respectively. Figures 6(e)–6(g) show the zoom-in view of the PSFs in regions [0, 1.5], [6.1, 7.6], and [12.4, 13.9], which cover the first period, the 6 dB sensitivity roll-off length, and the 20 dB sensitivity roll-off length, respectively. In Fig. 6(e), the PSFs have almost no degradation from 0 to 1.5 mm. The side-lobe suppression ratio is ~32 dB, and the signal-to-noise ratio is ~40 dB.

Figure 7 shows the typical interference signals and unwrapped PSFs of the OCT system with the microring comb filter. Since the sweep range is slightly reduced compared with Fig. 6, the axial resolution is measured to be 22 μm. As a result of the narrow linewidth, the 6 dB sensitivity roll-off length is extended to ~53 mm, which is 7.5 times that with the F–P comb filter. The enhancement of the sensitivity roll-off length by 7.5 times is in accordance with the linewidth narrowing from 12.1 to 1.5 GHz, which predicts an improvement of coherence length by ~8 times. Besides, the 10 dB sensitivity roll-off length is 73 mm, and the 15 dB roll-off length is more than 100 mm. The side-lobe suppression ratio is ~27 dB, and the signal-to-noise ratio is ~35 dB, which is slightly degraded compared with Fig. 6.

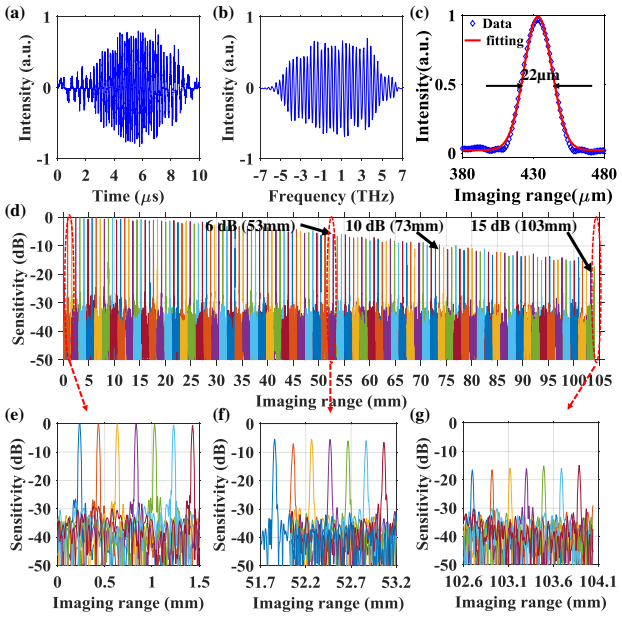

Fig. 7. (a) Example of raw interference fringe pattern with microring comb filter captured by the BPD. (b) Resampled interference spectrum with self-clocking. (c) Axial resolution estimation with PSF calculated from the signal of (b). (d)–(g) The measured PSFs of frequency comb swept laser with microring comb filter for different OCT imaging ranges. (d) The imaging range from 0 to 104 mm. (e) The zoom in view from 0 to 1.5 mm. (f) The zoom-in view from 51.7 to 53.2 mm, covering the 6 dB sensitivity roll-off length. (g) The zoom-in view from 102.6 to 104.1 mm, covering the 15 dB sensitivity roll-off length.

4. CONCLUSIONS

In summary, we have demonstrated a frequency comb swept laser based on a microring comb filter with a linewidth of ~90 MHz and a Q factor of $>2 \times 10^6$ in an FDML laser cavity. An F–P comb filter with a linewidth of ~3.1 GHz and a Q factor of $\sim 6.2 \times 10^4$ is used for comparison. The linewidth of the swept comb lines with the microring comb filter is narrowed to 1.5 GHz, which is only one-eighth of the linewidth with the F–P comb filter. The 6 dB sensitivity roll-off length of the OCT system with the microring-based frequency comb swept laser is extended to 53 mm, which is 7.5 times that with the F–P comb filter. To the best of our knowledge, this is the first time that the coherence length of FDML lasers is extended to 100 mm level. The 15 dB sensitivity roll-off length of OCT systems using such FDML sources will be enlarged to >100 mm. It is obvious that the ultralong coherence length obtained in the frequency comb swept laser is the direct consequence of the narrow linewidth of the microring comb filter. In addition, the identical frequency spacing of the discrete pulse signals can serve as the clock to realize time-to-frequency mapping, which simplifies the data acquisition and processing for the SS-OCT systems. The ultralong coherence length frequency comb swept laser will be a preferable choice for long-range OCT including circular interferometric imaging, which could greatly reduce the data volume for imaging at video rate.

Funding. Research Grants Council, University Grants Committee of Hong Kong SAR (PolyU152241/18E, PolyU152471/16E); Science, Technology and Innovation Commission of Shenzhen Municipality (JCYJ20160331 141313917, SGDX2019081623060558); The Hong Kong Polytechnic University (1-BBAJ, 1-ZVGB).

Disclosures. The authors declare no conflicts of interest.

REFERENCES

1. D.-P. Zhou, Z. Qin, W. Li, L. Chen, and X. Bao, "Distributed vibration sensing with time-resolved optical frequency-domain reflectometry," Opt. Express **20**, 13138–13145 (2012).
2. D. Chen, C. Shu, and S. He, "Multiple fiber Bragg grating interrogation based on a spectrum-limited Fourier domain mode-locking fiber laser," Opt. Lett. **33**, 1395–1397 (2008).
3. C.-Y. Ryu and C.-S. Hong, "Development of fiber Bragg grating sensor system using wavelength-swept fiber laser," Smart Mater. Struct. **11**, 468–473 (2002).
4. R. Huber, M. Wojtkowski, and J. G. Fujimoto, "Fourier domain mode locking (FDML): a new laser operating regime and applications for optical coherence tomography," Opt. Express **14**, 3225–3237 (2006).
5. R. Huber, M. Wojtkowski, K. Taira, J. G. Fujimoto, and K. Hsu, "Amplified, frequency swept lasers for frequency domain reflectometry and OCT imaging: design and scaling principles," Opt. Express **13**, 3513–3528 (2005).
6. M. Siddiqui, A. S. Nam, S. Tozburun, N. Lippok, C. Blatter, and B. J. Vakoc, "High-speed optical coherence tomography by circular interferometric ranging," Nat. Photonics **12**, 111–116 (2018).
7. T. Klein and R. Huber, "High-speed OCT light sources and systems [Invited]," Biomed. Opt. Express **8**, 828–859 (2017).
8. W. Wieser, W. Draxinger, T. Klein, S. Karpf, T. Pfeiffer, and R. Huber, "High definition live 3D-OCT *in vivo*: design and evaluation of a 4D OCT engine with 1 GVoxel/s," Biomed. Opt. Express **5**, 2963–2977 (2014).
9. J. Xu, X. Wei, L. Yu, C. Zhang, J. Xu, K. K. Y. Wong, and K. K. Tsia, "High-performance multi-megahertz optical coherence tomography based on amplified optical time-stretch," Biomed. Opt. Express **6**, 1340–1350 (2015).
10. A. F. Fercher, W. Drexler, C. K. Hitzenberger, and T. Lasser, "Optical coherence tomography—principles and applications," Rep. Prog. Phys. **66**, 239–303 (2003).
11. A.-H. Dhalla, D. Nankivil, and J. A. Izatt, "Complex conjugate resolved heterodyne swept source optical coherence tomography using coherence revival," Biomed. Opt. Express **3**, 633–649 (2012).
12. R. Huber, D. C. Adler, and J. G. Fujimoto, "Buffered Fourier domain mode locking: unidirectional swept laser sources for optical coherence tomography imaging at 370,000 lines/s," Opt. Lett. **31**, 2975–2977 (2006).
13. J. Zhang, J. Jing, P. Wang, and Z. Chen, "Polarization-maintaining buffered Fourier domain mode-locked swept source for optical coherence tomography," Opt. Lett. **36**, 4788–4790 (2011).
14. M. W. Jenkins, D. C. Adler, M. Gargesha, R. Huber, F. Rothenberg, J. Belding, M. Watanabe, D. L. Wilson, J. G. Fujimoto, and M. Rollins, "Ultrahigh-speed optical coherence tomography imaging and visualization of the embryonic avian heart using a buffered Fourier domain mode locked laser," Opt. Express **15**, 6251–6267 (2007).
15. J. P. Kolb, T. Pfeiffer, M. Eibl, H. Hakert, and R. Huber, "High-resolution retinal swept source optical coherence tomography with an ultra-wideband Fourier-domain mode-locked laser at MHz A-scan rates," Biomed. Opt. Express **9**, 120–130 (2018).
16. K. Hsu, P. Meemon, K.-S. Lee, P. J. Delfyett, and J. P. Rolland, "Broadband Fourier-domain mode-locked lasers," Photon. Sens. **1**, 222–227 (2011).
17. D. C. Adler, W. Wieser, F. Trepanier, J. M. Schmitt, and R. A. Huber, "Extended coherence length Fourier domain mode locked lasers at 1310 nm," Opt. Express **19**, 20930–20939 (2011).

18. W. Wieser, T. Klein, D. C. Adler, F. Trépanier, C. M. Eigenwillig, S. Karpf, J. M. Schmitt, and R. Huber, "Extended coherence length megahertz FDML and its application for anterior segment imaging," Biomed. Opt. Express **3**, 2647–2657 (2012).
19. T. Pfeiffer, M. Petermann, W. Draxinger, C. Jirauschek, and R. Huber, "Ultra low noise Fourier domain mode locked laser for high quality megahertz optical coherence tomography," Biomed. Opt. Express **9**, 4130–4148 (2018).
20. F. Li, K. Nakkeeran, J. N. Kutz, J. Yuan, Z. Kang, X. Zhang, and P. K. A. Wai, "Eckhaus instability in the fourier-domain mode locked fiber laser cavity," arXiv:1707.08304 (2017).
21. J. P. Kolb, W. Draxinger, J. Klee, T. Pfeiffer, M. Eibl, T. Klein, W. Wieser, and R. Huber, "Live video rate volumetric OCT imaging of the retina with multi-MHz A-scan rates," PLoS ONE **14**, e0213144 (2019).
22. N. Lippok, B. E. Bouma, and B. J. Vakoc, "Stable multi-megahertz circular-ranging optical coherence tomography at 13 μm," Biomed. Opt. Express **11**, 174–185 (2020).
23. T.-H. Tsai, C. Zhou, D. C. Adler, and J. G. Fujimoto, "Frequency comb swept lasers," Opt. Express **17**, 21257–21270 (2009).
24. S. Tozburun, M. Siddiqui, and B. J. Vakoc, "A rapid, dispersion-based wavelength-stepped and wavelength-swept laser for optical coherence tomography," Opt. Express **22**, 3414–3424 (2014).
25. T. Yang, X. Wei, C. Kong, S. Tan, K. K. M. Tsia, and K. K. Y. Wong, "An ultrafast wideband discretely swept fiber laser," IEEE J. Sel. Top. Quantum Electron. **24**, 8800105 (2018).
26. M. Wan, F. Li, X. Feng, X. Wang, Y. Cao, B. Guan, D. Huang, J. Yuan, and P. K. A. Wai, "Time and Fourier domain jointly mode locked frequency comb swept fiber laser," Opt. Express **25**, 32705–32712 (2017).
27. T. Herr, K. Hartinger, J. Riemensberger, C. Y. Wang, E. Gavartin, R. Holzwarth, M. L. Gorodetsky, and T. J. Kippenberg, "Universal formation dynamics and noise of Kerr-frequency combs in microresonators," Nat. Photonics **6**, 480–487 (2012).
28. D. T. Spencer, J. F. Bauters, M. J. R. Heck, and J. E. Bowers, "Integrated waveguide coupled Si_3N_4 resonators in the ultrahigh-*Q* regime," Optica **1**, 153–157 (2014).
29. X. Ji, F. A. S. Barbosa, S. P. Roberts, A. Dutt, J. Cardenas, Y. Okawachi, A. Bryant, A. L. Gaeta, and M. Lipson, "Ultra-low-loss on-chip resonators with sub-milliwatt parametric oscillation threshold," Optica **4**, 619–624 (2017).
30. W. Wang, Z. Lu, W. Zhang, S. T. Chu, B. E. Little, L. Wang, X. Xie, M. Liu, Q. Yang, L. Wang, J. Zhao, G. Wang, Q. Sun, Y. Liu, Y. Wang, and W. Zhao, "Robust soliton crystals in a thermally controlled microresonator," Opt. Lett. **43**, 2002–2005 (2018).
31. M. Peccianti, A. Pasquazi, Y. Park, B. E. Little, S. T. Chu, D. J. Moss, and R. Morandotti, "Demonstration of a stable ultrafast laser based on a nonlinear microcavity," Nat. Commun. **3**, 765 (2012).
32. D. J. Moss, R. Morandotti, A. L. Gaeta, and M. Lipson, "New CMOS-compatible platforms based on silicon nitride and Hydex for nonlinear optics," Nat. Photonics **7**, 597–607 (2013).
33. T. J. Kippenberg, R. Holzwarth, and S. A. Diddams, "Microresonator-based optical frequency combs," Science **332**, 555–560 (2011).
34. T. J. Kippenberg, A. L. Gaeta, M. Lipson, and M. L. Gorodetsky, "Dissipative Kerr solitons in optical microresonators," Science **361**, eaan8083 (2018).
35. D. K. Armani, T. J. Kippenberg, S. M. Spillane, and K. J. Vahala, "Ultra-high-*Q* toroid microcavity on a chip," Nature **421**, 925–928 (2003).
36. Z. Cen, F. Li, Q. Li, and P. K. A. Wai, "High quality pulse train from discrete Fourier domain mode locked laser with a comb filter," in *Asia Communications and Photonics Conference (ACP)* (2018), paper M1A.7.